J|A|C|S
ARTICLES
Published on Web 02/24/2007

From Single to Multiple Atomic Layers: A Unique Approach to the Systematic Tuning of Structures and Properties of Inorganic−Organic Hybrid Nanostructured Semiconductors

Xiaoying Huang and Jing Li*

Contribution from the Department of Chemistry and Chemical Biology, Rutgers University, Piscataway, New Jersey 08854

Received August 9, 2006; E-mail: jingli@rci.rutgers.edu

Abstract: In order to systematically tailor the structures and properties of a unique family of inorganic−organic hybrid nanostructured materials based on II−VI semiconductors, we have designed and engineered a new group of two-dimensional crystalline [(M_2Q_2)(L)] nanostreuctures (where M = Zn, Cd; Q = S, Se; and L = ethylamine, *n*-propylamine, *n*-butylamine, *n*-amylamine, *n*-hexylamine). These compounds are composed of double atomic layers of M_2Q_2 separated by organic monoamines. The crystal structures of 2D-[(M_2Q_2)(L)] are characterized by powder X-ray diffraction (PXRD) analysis. The crystal structures of these compounds are similar to the 2D-[(MQ)(L)] series that we reported earlier, in that they also contain II−VI slabs sandwiched by organic monoamines. The main difference is in the thickness of the II−VI slabs, where they are single-layer (n = 1) in 2D-[(MQ)(L)] but double-layer (n = 2) in 2D-[(M_2Q_2)(L)]. Optical absorption experiments show that all double-layer compounds exhibit a blue shift in their absorption edge (0.6−1.2 eV), due to the quantum confinement effect (QCE). However, the extent of such a blue shift is significantly less than that of the single-layer 2D-[(MQ)(L)] systems (1.0−2.0 eV) as a result of the difference in their layer thickness. Thermogravimetric (TG) analysis has revealed nanosized II−VI (MQ) particles as the post-TG product of all double-layer hybrids.

Introduction

II−VI binary chalcogenide compounds such as ZnS, ZnSe, and CdTe are of great fundamental and technological importance due to their superior properties and wide applications in semiconductor industries, including transistors, heterojunction diodes, space charge limited diodes, photoconductors, and photovoltaic devices.[1] Recent development on the synthesis and fabrication of nanoparticles of these semiconductors has created a new way to systematically tune their optical and electronic properties, simply by manipulating their physical dimensions.[2] Quantum dots grown by colloidal methods are particularly attractive because of their small size, narrow size distribution, size tunability, controllable morphology, and strong capability in modifying semiconductor bulk properties.[2]

Despite the remarkable success in the development of colloidal quantum dots, the generation of strongly correlated, uniform, and periodic lattices of dots remains a great challenge. Single-sized and uniformly arranged nanostructures having strong correlation in at least one dimension are most desirable for optical applications that require sharp line width and high intensity and for optoelectronic devices in which high conductivity/mobility is needed, such as high-efficiency transistors and solar cells. Therefore, it is essential to explore new types of nanostructures that possess these important features while having the same extent of tunability as those of colloidal quantum dots.

Scheme 1

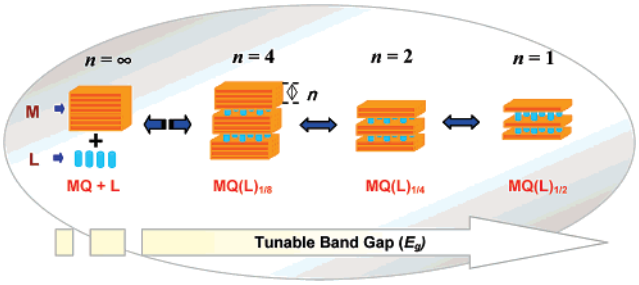

Our strategy to design nanostructured II−VI semiconductor materials has been to build crystalline lattices that consist of single-sized and periodic arrays of II−VI fragments at nanometer or subnanometer scale, which are interconnected or separated by suitable organic molecules via coordinative bonds.[3] These organic insulators act as spacers that prevent interactions among the neighboring inorganic fragments, thus inducing strong quantum confinement. We have successfully developed a unique class of structures of this type, namely, [$MQ(L)_x$] (where M = Mn, Zn, Cd; Q = S, Se, Te; and L = mono- or

(1) (a) Sze, S. M. *Semiconductor Devices: Physics and Technology*, 2nd ed.; Wiley: New York, 2001. (b) Ng, K. K. *Complete Guide to Semiconductor Devices*, 2nd ed.; Wiley−IEEE Press: New York, 2002. (c) Singh, J. *Semiconductor Optoelectronics: Physics and Technology*; McGraw-Hill: New York, 1995. (d) Neumark, G. F.; Park, R. M.; Depuydt, J. M. *Phys. Today* **1994** (June), 26. (e) McClean, I. P.; Thomas, C. B. *Semicond. Sci. Technol.* **1992**, *7*, 1394.

(2) (a) Alivisatos, A. P. *Science* **1996**, *271*, 933. (b) Murray, C. B.; Kagan, C. R.; Bawendi, M. G. *Science* **1995**, *270*, 1335. (c) Murray, C. B.; Norris, D. J.; Bawendi, M. G. *J. Am. Chem. Soc.* **1993**, *115*, 8706. (d) Trindade, T.; O'Brien, P.; Picket, N. L. *Chem. Mater.* **2001**, *13*, 3843. (e) Micic, O. I.; Cheong, H. M.; Fu, H.; Zunger, A.; Sprague, J. R.; Mascarenhas, A.; Nozik, A. J. *J. Phys. Chem. B* **199**7, *101*, 4904.

10.1021/ja065799e CCC: $37.00

Table 1. Summary of Reaction Conditions

2D compounds	starting materials	amount (mmol)	temp (°C)	time (days)
$[(Zn_2S_2)(ea)]$ (**1**)	$ZnCl_2$ + 1 mL of CS_2 + 4 mL of ea	4	60	5
$[(Zn_2S_2)(pa)]$ (**2**)	$2Zn(NO_3)_2{\cdot}6H_2O$ + S + 4 mL of pa	1	110	5
$[(Zn_2S_2)(ba)]$ (**3**)	$2ZnCl_2$ + S + 4 mL of ba	1	120	6
$[(Zn_2S_2)(aa)]$ (**4**)	$2ZnCl_2$ + S + 0.3 mL of aa	0.5	90	10
$[(Zn_2S_2)(ha)]$ (**5**)	$2ZnCl_2$ + S + 6 mL of ha	2	120	2
$[(Zn_2Se_2)(ea)]$ (**6**)	$2Zn(NO_3)_2{\cdot}6H_2O$ + Se + 10 mL of ea	4	150	6
$[(Zn_2Se_2)(pa)]$ (**7**)	$2Zn(NO_3)_2{\cdot}6H_2O$ + Se + 15 mL of pa	2	140	5
$[(Zn_2Se_2)(ba)]$ (**8**)	$2Zn(NO_3)_2{\cdot}6H_2O$ + Se + 15 mL of ba	2	140	5
$[(Zn_2Se_2)(aa)]$ (**9**)	$2ZnCl_2$ + Se + 0.4 mL of aa	0.5	120	7
$[(Zn_2Se_2)(ha)]$ (**10**)	$2ZnCl_2$ + Se + 10 mL of ha	2	140	5
$[(Cd_2S_2)(pa)]$ (**11**)	$2CdCl_2$ + S + 10 mL of pa	1	80	3
$[(Cd_2S_2)(ba)]$ (**12**)	$2CdCl_2$ + S + 12 mL of ba	2	80	4
$[(Cd_2S_2)(ha)]$ (**13**)	$1.5CdCl_2$ + S + 10 mL of ha	0.5	50	3
$[(Cd_2Se_2)(pa)]$ (**14**)	$Cd(NO_3)_2{\cdot}4H_2O$ + Se + 7 mL of pa	1	110	5
$[(Cd_2Se_2)(ba)]$ (**15**)	$Cd(NO_3)_2{\cdot}4H_2O$ + Se + 6 mL of ba	1	110	5
$[(Cd_2Se_2)(ha)]$ (**16**)	$2Cd(NO_3)_2{\cdot}4H_2O$ + Se + 5 mL of ha	1	120	6
[(ZnS)(ma)] (**17**)	$2ZnCl_2$ + S + 12 mL of ma	2	65	7
[(ZnS)(pa)] (**18**)	$2ZnCl_2$ + S + 10 mL of pa	1	60	3
[(ZnS)(ba)] (**19**)	$2ZnCl_2$ + S + 16 mL of ba	2	65	7
[(ZnS)(ha)] (**20**)	$2ZnCl_2$ + S + 16 mL of ba	2	65	7
[(ZnSe)(ma)] (**21**)	$2ZnCl_2$ + Se + 16 mL of ma	1	130	7
[(ZnSe)(ea)] (**22**)	$2ZnCl_2$ + Se + 8 mL of ea	1	120	8
[(ZnSe)(pa)] (**23**)	$2ZnCl_2$ + Se + 8 mL of pa	2	150	2
[(ZnSe)(ba)] (**24**)	$2ZnCl_2$ + Se + 4 mL of ba	1	140	7
[(ZnSe)(ha)] (**25**)	$2Zn(ClO_4)_2{\cdot}6H_2O$ + Se + 4 mL of ha	1	140	3

diamine molecules or hydrazine; $x = 0.5$ or 1), all of which are composed of single atomic layers or single atomic chains of II−VI nanocomponents.[3] These compounds exhibit significantly enhanced electronic and optical properties,[3−6] including a giant band gap tunability as a result of strong quantum confinement effect (QCE; blue shifts up to ∼2 eV) and high band-edge absorption (e.g., 10−20 times higher in 3D-$ZnTe(en)_{0.5}$ compared to bulk GaAs).[4a] Theoretical calculations on 3D-$[ZnTe(en)_{1/2}]$[3a,4b] and 3D-$[ZnSe(en)_{1/2}]$[5a] using density functional theory within local density approximation (LDA) as well as optical measurements[4] have verified that the observed large blue shifts in the band-edge absorption are primarily due to the strong quantum confinement effect in the II−VI semiconductor fragments of these hybrid materials. While the extent of band-gap variation is significantly greater than what has been achieved for the smallest colloidal quantum dots (∼1 eV), the hybrid materials have additional advantage of possessing perfectly ordered crystal structures and thus allowing high carrier mobility. Our study also illustrates a significant reduction of lattice mismatch in these systems, which is highly advantageous for applications in multijunction solar cells. Furthermore, the hybrid crystals are much lighter and more flexible compared with their inorganic counterparts, and thus are most desirable for low-weight and flexible photovoltaic devices.

An interesting structure−property correlation can be derived on the basis of our knowledge of the single-layer II−VI hybrid structures. As shown in Scheme 1, variation of a single structure parameter, the thickness n of a II−VI MQ slab (shown in orange), can lead to systematic tuning of band gap. The structure of a II−VI bulk (zinc-blende or wurtzite) is sketched at the left side where $n = \infty$. At the right side is the 3D-$[MQ(L)_{0.5}]$ structure where $n = 1$ (single atomic layer). They represent the two extreme cases with zero ($n = \infty$) and strongest ($n = 1$) quantum confinement, respectively. Clearly, construction of hybrid structures having intermediate n between the two extreme cases will allow controllable and systematic tuning of the band gap and thus the electronic and optical properties. Two intermediate cases are also shown in Scheme 1, as $n = 2$ (double-layer) and $n = 4$ (quadruple-layer).

In this work, we report the design and synthesis, crystal structure characterization, and optical and thermal properties of the $n = 2$ subgroup, $[(M_2Q_2)(L)]$ (where M = Cd, Zn; Q = S, Se; and L = ethylamine, *n*-propylamine, *n*-butylamine, *n*-amylamine, *n*-hexylamine), of the II−VI-based hybrid semiconductor family; all are composed of double-layered $[M_2Q_2]$ slabs and monoamine organic spacers.

Experimental Section

Materials and Instruments. $ZnCl_2$ (98%, Aldrich), $Zn(NO_3)_2{\cdot}6H_2O$ (97%, Alfa Aesar), $Zn(ClO_4)_2{\cdot}6H_2O$ (reagent grade, Alfa Aesar), $CdCl_2$ (99.9%, Strem), $Cd(NO_3)_2{\cdot}4H_2O$ (98.5%, Alfa Aesar), Se (99.5%, Strem), S (98%, Strem), CS_2 (99.0%, Aldrich), methylamine (ma, 40%, aqueous solution, Alfa Aesar), ethylamine (ea, 70%, aqueous solution, Alfa Aesar), *n*-propylamine (pa, 99%, Alfa Aesar), *n*-butylamine (ba, 99%, Alfa Aesar), *n*-amylamine (aa, 99%, Aldrich), and *n*-hexylamine (ha, 99%, Alfa Aesar) were used as received without further purification. Powder X-ray diffraction (PXRD) of samples was performed on a Rigaku D/M-2200T automated diffraction system (Ultima$^+$). Optical diffuse reflectance spectra were measured at room temperature on a Shimadzu UV-3101PC double-beam, double-monochromated spectrophotometer. Thermogravimetric analysis (TGA) was performed on a computer-controlled TA Instrument TG Q50 system.

Synthesis. Solvothermal reactions were performed in either acid digestion bombs (23 or 50 mL) or Pyrex tubes. The solid reactants were weighed and transferred to the reaction vessels, followed by

(3) (a) Huang, X.-Y.; Li, J.; Fu, H. *J. Am. Chem. Soc.* **2000**, *122*, 8789. (b) Huang, X. Y.; Heulings, H. R., IV; Le, V.; Li, J. *Chem. Mater.* **2001**, *13*, 3754. (c) Heulings, H. R., IV; Huang, X.-Y.; Li, J.; Yuen, T.; Lin, C. L. *Nano Lett.* **2001**, *10*, 521. (d) Huang, X.-Y.; Li, J. *Mater. Res. Soc. Symp. Proc.* **2002**, *728*, 17. (e) Huang, X.-Y.; Li, J.; Zhang, Y.; Mascarenhas, A. *J. Am. Chem. Soc.* **2003**, *125*, 7049. (f) Huang, X.-Y.; Heulings, H. R., IV; Li, J.; Yuen, T.; Lin, C. L. *J. Nanosci. Nanotechnol.* **2005**, *5*, 1487.
(4) (a) Fluegel, B.; Zhang, Y.; Mascarenhas, A.; Huang, X.-Y.; Li, J. *Phys. Rev. B* **2004**, *70* (20), 205308/1. (b) Zhang, Y.; Dalpian, G. M.; Fluegel, B. Wei, S.-H.; Mascarenhas, A.; Huang, X.-Y.; Li, J.; Wang, L.-W. *Phys. Rev. Lett.* **2006**, *96*, 026405.
(5) (a) Fu, H.-X.; Li, J. *J. Chem. Phys.* **2004**, *14*, 6721. (b) Moon, C.-Y.; Dalpian, G. M.; Zhang, Y.; Wei, S.-H.; Huang, X.-Y.; Li, J. *Chem. Mater.* **2006**, *18*, 2805.
(6) (a) Lu, J.; Wei, S.; Peng, Y.-Y.; Yu, W.-C.; Qian, Y.-T. *J. Phys. Chem. B* **2003**, *107*, 3427. (b) Lu, J.; Wei, S.; Yu, W.-C.; Zhang, H.-B.; Qian, Y.-T. *Chem. Mater.* **2005**, *17*, 1698.

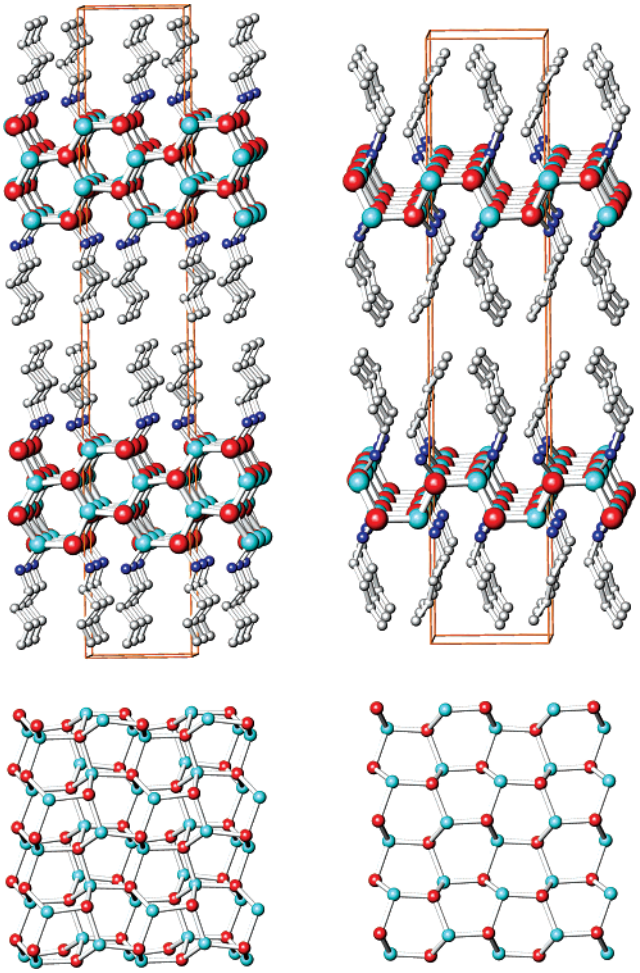

Figure 1. Top left: crystal structure of double-layer 2D-[(Zn_2Se_2)(ba)] (**8**) viewed along the *b*-axis. The light blue balls are Zn; red balls, Se; blue balls, N; gray balls, C. Hydrogen atoms are omitted for clarity. Top right: crystal structure of single-layer 2D-[(ZnSe)(ba)] (**24**) viewed along the *b*-axis. Bottom left: double atomic layer of [Zn_2Se_2] of **8** shown along the *ab* plane. Bottom right: single atomic layer of [ZnSe] of **24** shown along the *ab* plane. Details of the Rietveld refinements as well as crystal data for both compounds can be found in Table S2−-1 and atomic positions are given in Table S2−-2, Supporting Information.

injection of solvents. The vessels were then sealed and heated in ovens at elevated temperatures. The vessels were naturally cooled down to room temperature after the reactions were complete. The final products were washed by 95% ethanol, 30% ethanol, and distilled water, respectively. The samples were further dried in anhydrous ethyl ether. The reaction conditions for the synthesis of each compound are summarized in Table 1. Further details can be found in Supporting Information (S3).

Powder X-ray Diffraction. Powder X-ray diffraction (PXRD) patterns of all compounds (**1**−**25**) (Table 1) were obtained from a Rigaku D/M-2200T automated diffraction system (Ultima$^+$) with Cu Kα radiation. Measurements were made in a 2θ range of 3−60°. The data were collected at room temperature with a step size of 0.02° (2θ) and a counting time of 0.2 s/step. The operating power was 40 kV/40 mA. Data used for the Rietveld refinement of a double-layer 2D-[(Zn_2Se_2)(ba)] (**8**) structure were collected on a National Synchrotron Light Source (λ = 0.619 332 Å) with an image plate detector (2θ range 1−31.5°). For the single-layer 2D-[ZnSe(ba)] (**24**) structure, data used in Rietveld refinement were obtained at room temperature on the Rigaku system (2θ range 3−100°, step size 0.01°, and counting time 8 s/step).

Thermal Analysis. Thermogravimetric (TG) analyses of the title compounds were performed on a computer-controlled TA Instrument TG Q50 analyzer. Single-phased powder samples were loaded into platinum pans and heated with a ramp rate of 5 °C/min from room temperature to ∼430 °C.

Diffuse Reflectance Measurements. Optical diffuse reflectance spectra were measured at room temperature with a Shimadzu UV-3101PC double-beam, double-monochromator spectrophotometer. Data were collected in the wavelength range of 250−2000 nm. $BaSO_4$ powder was used as a standard (100% reflectance). A similar procedure as previously described[7] was used to collect and convert the data by use of the Kubelka−Munk function.[8] The scattering coefficient (*S*) was treated as a constant since the average particle size of the samples used in the measurements was significantly larger than 5 μm.

Results and Discussion

Synthesis. All compounds adopting a double-layered structure 2D-[(M_2Q_2)(L)] (M = Zn, Cd; Q = S, Se; L = monoamines) were obtained via solvothermal reactions using monoamines as solvents as well as reactive reagents. All reactions were carried out under relatively mild conditions (50−160 °C), as shown below:

$$Zn^{2+} + S + L \rightarrow [Zn_2S_2(L)]\ (L = ea, pa, ba, aa, ha)$$

$$Zn^{2+} + Se + L \rightarrow [Zn_2Se_2(L)]\ (L = ea, pa, ba, aa, ha)$$

$$Cd^{2+} + S + L \rightarrow [Cd_2S_2(L)]\ (L = pa, ba, ha)$$

$$Cd^{2+} + Se + L \rightarrow [Cd_2Se_2(L)]\ (L = pa, ba, ha)$$

Temperature played a crucial role in the synthesis. Three competitive products were found from these reactions: double-layer 2D-[(M_2Q_2)(L)], single-layer 2D-[(MQ)(L)],[3e] and II−VI binary phases. By carefully selecting a suitable temperature range, we succeeded in isolating single-phase product for each system. Normally higher temperature favored the formation of binary MQ, while at intermediate temperature double-layered 2D-[(M_2Q_2)(L)] became the major phase. At lower temperature, only single-layered 2D-[(MQ)(L)] phases were formed. For double-layer 2D-[(M_2Q_2)(L)] hybrids based on different II−VI (MQ) system, the single-phase samples were obtained at different temperatures. For example, pure [(Zn_2S_2)(L)] were obtained between 60 and 120 °C, while single-phase isostructural [(Zn_2Se_2)(L)] compounds were prepared at 120−150 °C. Similarly, [(Cd_2Se_2)(L)] samples were obtained at 110−120 °C, while milder conditions (50−80 °C) were required for the synthesis of CdS-based double-layered hybrid compounds. Binary II−VI compounds became the major products for temperatures above 160 °C.

Structure Characterization. All compounds (**1**−**25**) were structurally characterized by powder X-ray diffraction (PXRD) methods. The double-layer 2D-[(Zn_2Se_2)(ba)] (**8**) structure crystallizes in orthorhombic crystal system, space group *Pbca*. The cell parameters of **8** were obtained from a full indexing of PXRD data, with a = 6.8035(9), b = 6.5194(6), and c = 41.894-(6) Å. The details of the Rietveld refinements, as well as crystal data, are listed in Table S2-1, and positional parameters are

(7) Li, J.; Chen, Z.; Wang, X.-X.; Proserpio, D. M. *J. Alloys Compd.* **1997**, *262*−*263*, 28.
(8) Wendlandt, W. W.; Hecht, H. G. *Reflectance Spectroscopy*; Interscience, A Division of John Wiley & Sons: New York, 1966.

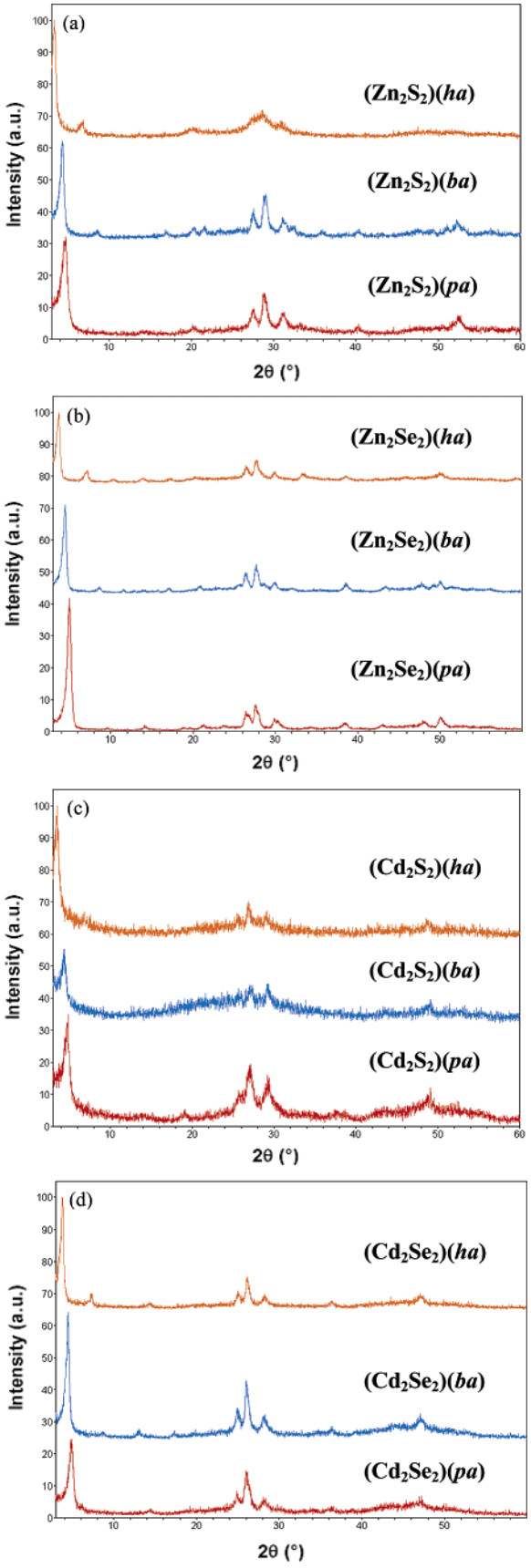

Figure 2. PXRD patterns of double-layer hybrid structures: (a) [(Zn_2S_2)(pa)] (**2**), [(Zn_2S_2)(ba)] (**3**), and [(Zn_2S_2)(ha)] (**5**); (b) [(Zn_2Se_2)(pa)] (**7**), [(Zn_2Se_2)(ba)] (**8**), and [(Zn_2Se_2)(ha)] (**10**); (c) [(Cd_2S_2)(pa)] (**11**), [(Cd_2S_2)(ba)] (**12**), and [(Cd_2S_2)(ha)] (**13**); (d) [(Cd_2Se_2)(pa)] (**14**), [(Cd_2Se_2)(ba)] (**15**), and [(Cd_2Se_2)(ha)] (**16**).

Table 2. PXRD Refined Unit Cell Paramenters of Selected Compounds[a]

compound	*a* (Å)	*b* (Å)	*c* (Å)
[ZnS(ma)]	6.415(3)	6.194(4)	20.296(11)
[ZnSe(ma)]	6.7099(17)	6.4786(17)	19.6134(5)
[ZnSe(ea)]	6.7312(13)	6.4952(9)	24.242(4)
[ZnSe(pa)]	6.687(2)	6.492(3)	30.289(10)
[ZnSe(ba)]	6.6746(17)	6.4642(10)	34.217(5)
[ZnSe(ha)]	6.686(2)	6.4724(19)	44.161(11)

[a] Selected single-layer 2D compounds [ZnQ(L)] (where Q = S, Se; and L = ma, ea, pa, ba, and ha).

Table 3. Band Gap and Blue Shift Values of Selected Compounds[a]

compound	BG (eV)	BS (eV)	compound	BG (eV)	BS (eV)
(Zn_2S_2)(ea)	4.0	0.8			
(Zn_2S_2)(pa)	3.9	0.7			
(Zn_2S_2)(ba)	3.9	0.7	(ZnS)(ba)	4.5	1.3
(Zn_2S_2)(aa)	4.0	0.8			
(Zn_2S_2)(ha)	4.0	0.8			
(Zn_2Se_2)(ea)	3.5	1.0			
(Zn_2Se_2)(pa)	3.5	1.0			
(Zn_2Se_2)(ba)	3.5	1.0	ZnSe(ba)	4.1	1.6
(Zn-$_2Se_2$)(aa)	3.5	1.0			
(Zn_2Se_2)(ha)	3.5	1.0			
(Cd_2S_2)(pa)	2.9	0.6			
(Cd_2S_2)(ba)	2.9	0.6	$CdS(pda)_{1/2}$	4.0	1.7
(Cd_2S_2)(ha)	2.9	0.6			
(Cd_2Se_2)(pa)	2.7	1.2			
(Cd_2Se_2)(ba)	2.7	1.2	$CdSe(pda)_{1/2}$	3.5	2.0
(Cd_2Se_2)(ha)	2.7	1.2			

[a] Band gap (BG) and blue shift (BS) values of selected double-layer 2D-[M_2Q_2(L)] compounds are compared with those of single-layer [MQ(L)*x*] (where M = Zn, Cd; Q = S, Se; and L = ea, pa, ba, ha, aa, and pda (1,3-propanediamine)). Estimated band gaps for II−VI bulk materials: CdS (wurtzite structure), 2.3 eV; CdSe (wurtzite structure), 1.5 eV; ZnS (zinc blende structure), 3.2 eV; ZnSe (zinc blende structure), 2.5 eV.

tabulated in Table S2-2, Supporting Information. Compared to that of the single-layer 2D-[ZnSe(ba)] (**24**), a = 6.6746(11), b = 6.4642(10), and c = 34.217(5) Å, the main difference is the length of the *c*-axis. As illustrated in Figure 1, the structure of **8** (Figure 1, left) is composed of double-layer [Zn_2Se_2] slabs (n = 2) rather than the single-layer [ZnSe] slabs (n = 1) as in **24** (Figure 1, right). In both structures, the slabs are sandwiched by coordinated *n*-butylamine layers. All Zn atoms have tetrahedral coordination. In **8**, there are two crystallographic independent Zn atoms. One bonds to four Se atoms to form a distorted tetrahedron. Another coordinates to three Se atoms and to one N atom of *n*-butylamine molecule. There are also two crystallographic independent Se atoms. One is tetrahedrally coordinated to four Zn atoms while the other is bound to three Zn atoms. The double-layer [Zn_2Se_2] slab (Figure 1, bottom left) can also be regarded as a "slice" cut from the (110) crystal face of the hexagonal ZnSe (or würtzite structure, constructed of both boat-shaped and chair-shaped six-membered rings). The thickness of the double-layer [Zn_2Se_2] slab is ~8.5 Å (using covalent radius of Se, 1.17 Å), falling well in the nano region. PXRD patterns displayed in Figure 2 indicate that all 2D-[(M_2Q_2)(L)] (M = Zn, Cd; Q = S, Se; and L = pa, ba, ha) compounds are isostructural to each other. As the length of the amines increases from *n*-propylamine (pa) to *n*-butylamine (ba) to *n*-hexylamine (ha), the first peaks of their PXRD patterns shift to lower 2θ diffraction angles.

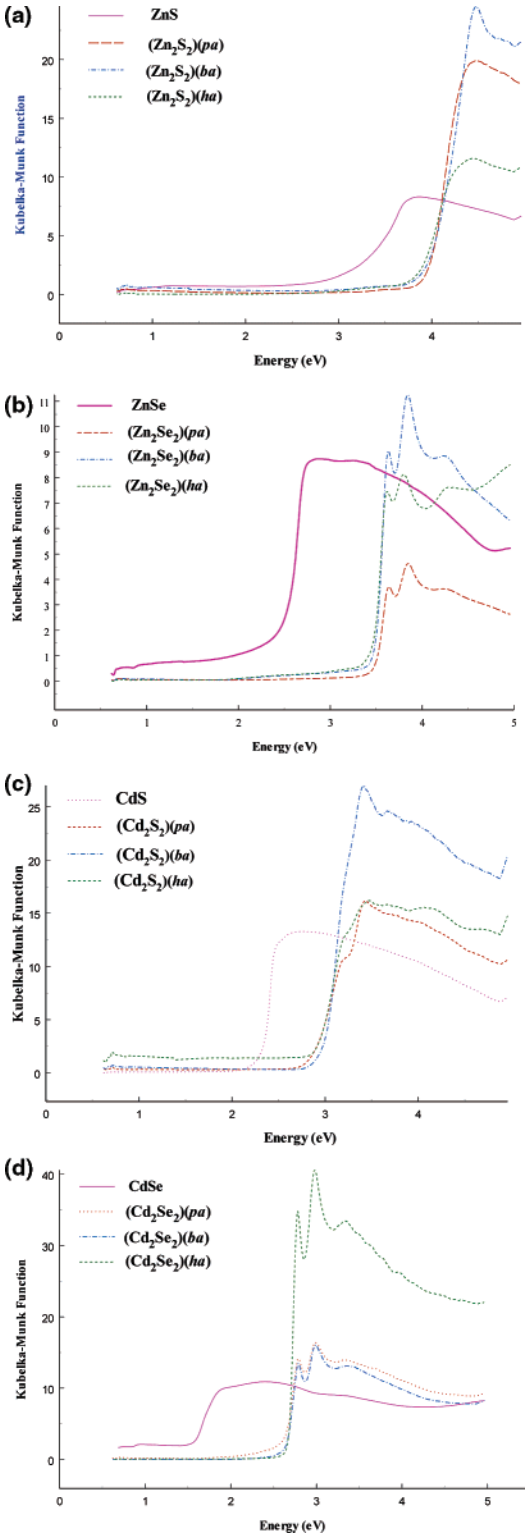

Figure 3. Optical absorption spectra: (a) [(Zn_2S_2)(pa) (**2**)] (red), [(Zn_2S_2)(ba)] (**3**) (blue), [(Zn_2S_2)(ha)] (**5**) (green), and bulk ZnS (pink). The estimated band gap for ZnS is 3.2 eV, and the onset absorption occurs at 3.9, 3.9, and 4.0 eV for **2**, **3**, and **5**, respectively. (b) [(Zn_2Se_2)(pa)] (**7**) (red), [(Zn_2Se_2)(ba)] (**8**) (blue), [(Zn_2Se_2)(ha)] (**10**) (green), and bulk ZnSe (pink). The estimated band gap for ZnSe is 2.5 eV, and the onset absorption occurs at 3.5 eV for **7**, **8**, and **10.** (c). [(Cd_2S_2)(pa)] (**11**) (red), [(Cd_2S_2)(ba)] (**12**) (blue), [(Cd_2S_2)(ha)] (**13**) (green), and bulk CdS (pink). The estimated band gap for CdS is 2.3 eV, and the onset absorption occurs at 2.9 eV for **11**, **12**, and **13.** (d) [(Cd_2Se_2)(pa)] (**14**) (red), [(Cd_2Se_2)(ba)] (**15**) (blue), [(Cd_2Se_2)(ha)] (**16**) (green), and bulk CdSe (pink). The estimated band gap for CdSe is 1.5 eV, and the onset absorption occurs at 2.7 eV for **14**, **15**, and **16**.

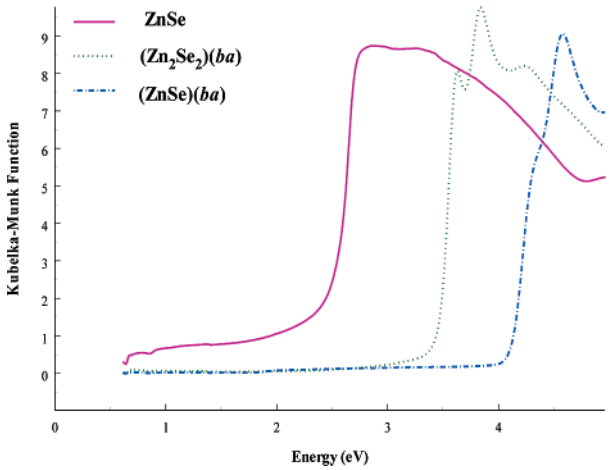

Figure 4. Optical absorption spectra of double-layer 2D-[(Zn_2Se_2)(ba)] (**8**) and single-layer 2D-[(ZnSe)(ba)] (**24**), along with that of ZnSe bulk (zinc blende structure). The estimated band gaps are 3.5, 4.1, and 2.5 eV, respectively.

The crystal structure analysis of the single-layer ($n = 1$) 2D-[(ZnSe)(ba)] (**24**) was also conducted by powder X-ray diffraction methods. Details of the GSAS refinements are depicted in Supporting Information (Table S2-1 and S2-2). The crystal structure of **24** (Figure 1, right) is similar to that of 2D-[ZnTe(ma)],[3e] which was determined by single-crystal X-ray diffraction methods. It crystallizes in orthorhombic crystal system (space group *Pbca*). There is only one type of Zn and it is coordinated to three Se and one N. The structure is composed of single-layered [ZnSe] slabs that are bonded to butylamine molecules from both sides of the slabs. The thickness of the single-layer [ZnSe] slab is ~4.8 Å. The unit cell parameters of **24**, along with several other isostructural single-layered 2D-[ZnQ(L)] (Q = S, Se; L = ma, ea, pa, ba, and ha) obtained from the indexing of their PXRD patterns, are listed in Table 2.

Optical Absorption and Band Gaps. The room-temperature optical absorption spectra of the double-layer hybrid compounds were obtained from diffuse reflectance experiments,[7,8] and the results are depicted in Figure 3, along with those of the parent binary MQ bulk. The absorption edges for [(Zn_2S_2)(pa)] (**2**), [(Zn_2S_2)(ba)] (**3**), and [(Zn_2S_2)(ha)] (**5**) are found to be 3.9−4.0 eV (Figure 3a). Compared to the measured value of 3.2 eV for zinc blende ZnS, it clearly indicates a blue shift of 0.7−0.8 eV. The optical properties of [(Zn_2Se_2)(pa)] (**7**), [(Zn_2Se_2)(ba)] (**8**), and [(Zn_2Se_2)(ha)] (**10**) were also assessed by the same experiments conducted at room temperature. As shown in Figure 3b, the estimated absorption edges are 3.5 eV for all three compounds. Compared to ~2.5 eV measured for the ZnSe bulk sample (zinc blende structure), the blue shifts are as large as 1.0 eV. The estimated absorption edges for [(Cd_2S_2)(pa)] (**11**), [(Cd_2S_2)(ba)] (**12**), and [(Cd_2S_2)(ha)] (**13**) are 2.9 eV, showing a blue shift of 0.6 eV compared to the bulk CdS (wurtzite structure) (Figure 3c). For [(Cd_2Se_2)(pa)] (**14**), [(Cd_2Se_2)(ba)] (**15**), and [(Cd_2Se_2)(ha)] (**16**), the blue shifts of the absorption edges are 1.2 eV (Figure 3d). Previous band structure and transition probability calculations on the single-layer 3D structures α-[ZnTe(en)$_{1/2}$],[3a,4b] β-[ZnTe(en)$_{1/2}$],[4b] and α-[ZnSe(en)$_{1/2}$][4b,5] employing density functional theory within local density approximation (LDA) have verified that the observed large blue shifts in the optical absorption spectra are due to

Table 4. Thermogravimetric Data Analysis for Selected Structures[a]

compound	WL % (calcd)	WL % (exptl)	T_d (°C)	residue
[(Zn_2S_2)(pa)] (**2**)	23.26	26.93	156/263	ZnS(w)
[(Zn_2S_2)(ba)] (**3**)	27.28	27.35	187/248	ZnS(w)
[(Zn_2S_2)(ha)] (**5**)	34.14	35.58	145/238	ZnS(w)
[(Zn_2Se_2)(pa)] (**7**)	16.99	18,68	181/262	ZnSe(w)
[(Zn_2Se_2)(ba)] (**8**)	20.21	21.43	180/257/315	ZnSe(w)
[(Cd_2S_2)(pa)] (**11**)	16.98	18.49	201	CdS(w)
[(Cd_2Se_2)(pa)] (**14**)	13.38	12.55	181	CdSe(w)
[(Cd_2Se_2)(ba)] (**15**)	16.03	16.23	193	CdSe(w)
[(Cd_2Se_2)(ha)] (**16**)	20.69	22.15	214	CdSe(w)

[a] Selected double-layer 2D structures [(M_2Q_2)(L)] (where M = Zn, Cd; Q = S, Se; and L = pa, ba, and ha) were studied. T_d = decomposition temperature; w = wurtzite structure; WL = weight loss.

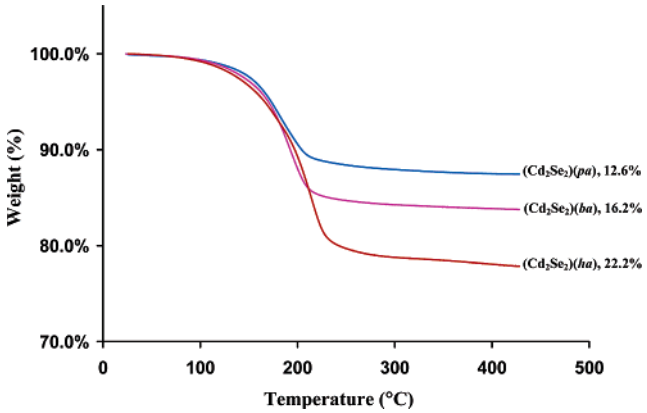

Figure 5. TG profiles for [(Cd_2Se_2)(pa)] (**14**), [(Cd_2Se_2)(ba)] (**15**), and [(Cd_2Se_2)(ha)] (**16**).

strong quantum confinement effect (QCE) in the II−VI single atomic layers in these hybrid materials. Density of states (DOS) analysis has revealed that the atomic states that contribute to the observed band-edge absorption are dominantly from the II/VI elements. Clearly, the band-edge shifts in the double-layer 2D-[(M_2Q_2)(L)] structures are significantly smaller than those of the corresponding single-layer 2D-[(MQ)(L)] compounds (see Table 3 and Supporting Information). This is because the extent of QCE is less in the former than in the latter. As shown in Scheme 1, the strongest confinement is achieved in the single-layer (n = 1) structures such as 2D-[(MQ)(L)]. As the layer thickness increases, the extent of QCE decreases, as does the blue shift in their band-edge absorption. Thus, for n = 1 (layer thickness ∼ 4.8 Å) as in a single-layered 2D-[(ZnSe)(ba)] (**24**) and n = 2 (layer thickness ∼ 8.5 Å) as in a double-layered 2D-[(Zn_2Se_2)(ba)] (**8**), the blue shifts are ∼1.6 and 1.0 eV, respectively (Figure 4).

Thermal Properties. The thermogravimetric (TG) analyses were performed on selected polycrystalline samples of double-layer 2D-[(M_2Q_2)(L)] hybrids, and the results are summarized in Table 4. As an illustrative example, Figure 5 shows the weight losses observed for [(Cd_2Se_2)(pa)] (**14**), [(Cd_2Se_2)(ba)] (**15**), and [(Cd_2Se_2)(ha)] (**16**) as a function of temperature between room temperature and 430 °C. All three compounds were thermally stable up to 100 °C. The decomposition occurred at ∼181−214 °C through a single-step weight-loss process. The measured weight losses of the organic species are 12.6% for pa in **14**, 16.2% for ba in **15**, and 22.2% for ha in **16**, respectively, in reasonable agreement with the calculated values of 13.4% for pa, 16.0% for ba, and 20.7% for ha, respectively. Powder X-ray diffraction analysis immediately following the TG experiments showed that the residues of all samples are nanoparticles of CdSe of würtzite structure. Similar behavior was observed for the [Cd_2S_2(L)] structures. [(Zn_2Se_2)(pa)] (**7**) and [(Zn_2Se_2)(ba)] (**8**) underwent two- and three-step decomposition between room temperature and ∼ 400 °C, with an onset decomposition temperature of ∼180 °C. Compared to the single-layer 2D-[(ZnSe)(L)], the decomposition temperatures of the double-layer hybrids are slightly lower (see Supporting Information). The weight losses are slightly higher than the calculated amount of monoamines, due possibly to the surface solvent. The post-TGA residuals were found to be würtzite ZnSe. [(Zn_2S_2)(pa)] (**2**), [(Zn_2S_2)(ba)] (**3**), and [(Zn_2S_2)(ha)] (**5**) also adopted a two-step weight loss process from room temperature to 420 °C. The experimental weight losses are in approximate agreement with the calculated weight of corresponding organic monoamines, while the post-TGA products are pure würtzite ZnS. Note that the decomposition temperatures of double-layer 2D-[(Zn_2S_2)-(monoamine)] are comparable to those of single-layer 2D-[ZnS-(monoamine)] but slightly lower than those of single-layer 3D-[ZnS($diamine)_{1/2}$].[3e]

Summary

A new series of inorganic−organic II−VI hybrid semiconductors with a general formula of 2D-[(M_2Q_2)(L)] (M = Zn, Cd; Q = S, Se; and L = ea, pa, ba, aa, and ha) have been designed and synthesized. The crystal structures of these compounds have a very similar topology as those of 2D-[(MQ)-(L)], but their 2D inorganic slabs are a double atomic layer of M_2Q_2 (n = 2), rather than a single atomic layer of MQ (n = 1) as in the 2D-[(MQ)(L)] structures. As in the case of the single-layer hybrid structures, a strong blue shift is observed in the optical absorption edges (band gaps) of all double-layer 2D-[(M_2Q_2)(L)] compounds as a result of strong quantum confinement effect, although the values of such a blue shift are smaller because the confinement in the II−VI slabs is less for n = 2 than for n = 1. The results from both optical measurements and thermal analysis are in excellent agreement with the structure proposed. The success in preparing the double-layer 2D-[M_2Q_2](L) structures serves as a beautiful example of structure−property correlation and illustrates how physical properties may be tuned systematically on the basis of the principles of quantum confinement effect and by modification of the crystal structures.

Acknowledgment. Financial support from the National Science Foundation (Grant DMR-0422932) is gratefully acknowledged. We thank Dr. Peter Lee (Argonne National Laboratory) for helpful discussions and for the use of the National Synchrotron Light Source.

Supporting Information Available: PXRD patterns, UV−vis spectra, and TGA results for single-layer 2D-[(MQ)(L)] structures and PXRD structure refinement details for compounds **8** and **24**. This material is available free of charge via the Internet at http://pubs.acs.org.

JA065799E